ISSN 1063-7745, Crystallography Reports, 2021, Vol. 66, No. 7, pp. 1206–1215. © Pleiades Publishing, Inc., 2021.

REAL STRUCTURE OF CRYSTALS

Crystallographic Parameters of Special Grain Boundaries in Multicrystalline Silicon

A. G. Chueshova[a,*], L. A. Pavlova[a], S. M. Peshcherova[a], and A. I. Nepomnyashchikh[a]

[a] *Vinogradov Institute of Geochemistry, Siberian Branch of the Russian Academy of Sciences, Irkutsk, 664033 Russia*

**e-mail: a.chueshova@igc.irk.ru*

Received October 21, 2020; revised November 18, 2020; accepted November 19, 2020

Abstract—The orientation of grains and the special boundaries formed by them in multicrystalline silicon has been studied by electron backscattered diffraction. It is found that the crystallographic parameters of special boundaries (misorientation angle and rotation axis) obtained using the Tango HKL Channel 5 software module may differ from the results of their direct computation by calculating the rotation matrix in the Spyder integrated development environment, using identical formulas based on Euler angles. In particular, special boundaries $\sum 3$, $\sum 9$, and $\sum 27a$ with misorientation angles of 180°, 120°, and 165°, respectively, are found in multicrystalline silicon. These versions of special grain boundaries are theoretically possible for the crystals of cubic system; however, they have not been investigated experimentally in multicrystalline silicon.

DOI: 10.1134/S106377452107004X

INTRODUCTION

Modern research in the field of solar power engineering is aimed, on the one hand, at developing the cheapest fabrication technologies of materials for photovoltaic converters and, on the other hand, at improving the quality of these materials. For example, the multicrystalline silicon based on high-purity metallurgical silicon (the so-called upgraded metallurgical grade (UMG) silicon) is a promising material for solar power engineering, and the efficiency of modern solar cells based on it reaches 22.6% [1]. However, the impurities present in the starting UMG silicon, being incorporated into multicrystalline silicon during crystallization, determine to a great extent the formation of the ingot macrostructure and, correspondingly, the bulk distribution of electrical properties. A particular role in the recombination of nonequilibrium carriers is played by intergrain boundaries, both of random and special types (special-type boundaries are grain boundaries with a periodic structure), since they all are efficient (but to different extents) sinks for the impurities responsible for the formation of deep levels [2]. The special boundaries with low inverse density of coinciding sites ($\sum < 27$) in the multicrystalline silicon grown from electronic quality silicon are considered to be most defect-free and, therefore, electrically neutral [3]. At the same time, impurities of transition metals (Fe, Ni, and Cu) in multicrystalline silicon obtained from UMG silicon affect significantly the intergrain boundaries, as a result of which special boundaries may exhibit recombination activity as high as 9% [4, 5]. However, the ability to impurity segregation is manifested by only incoherent special grain boundaries (GBs) consisting of facets, with dislocations enclosed between them [6]. According to the data in the literature, special GBs in the multicrystalline silicon obtained from electronic-quality silicon and from UMG silicon may differ in the degree of recombination activity due to their interaction with impurities and dislocations; however, their structure is retained [7]. To date, all types of special GBs and their crystallographic parameters in multicrystalline silicon have been experimentally discovered and studied [8]. Nevertheless, according to the results of numerical simulation, there are much more versions for the family of cubic crystals [9, 10]. In addition, Lazebnykh and Mysovsky [11] presented a model of special grain boundaries, constructed by the method of classical molecular mechanics for multicrystalline silicon, with misorientation angles and rotation axes differing from those reported in [7, 12–14].

The reasons for which these boundaries had not been detected previously in electron backscattered diffraction experiments may be as follows. On the one hand, it is the absence of all possible crystallographic parameters (rotation axis–misorientation angle pairs) in the Tango HKL Channel 5 software library. On the other hand, the multicrystalline silicon under study has individual features due to the impurity composition and conditions of Bridgman directional solidification. In this study, the crystallographic parameters of GBs (misorientation angle–rotation axis pairs) and grains (Miller indices of crystallographic planes) were calculated in two ways. The presented method for calculating these parameters implies construction of

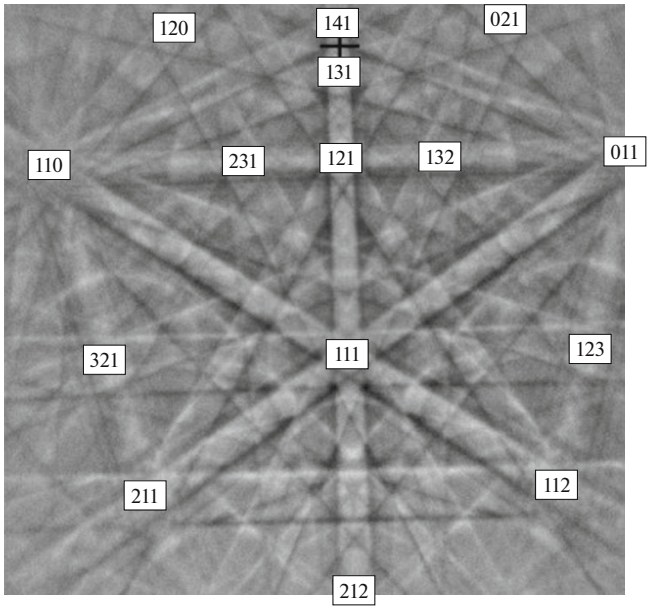

Fig. 1. Example of Kikuchi pattern indexing [15].

rotation matrices (what is meant is the rotation of one grain relative to another) in the scientific Python development environment Spyder, based on theoretically derived formulas. To obtain the Euler angles for each grain, which are necessary to calculate the rotation matrix, electron backscattered diffraction analysis was performed using the Tango HKL Channel 5 software module. The second method implies only determination of all crystallographic parameters applying the Tango HKL Channel 5 software.

MATERIALS AND METHODS OF STUDY

Electron Backscattered Diffraction

The electron backscattered diffraction method is based on the identification of Kikuchi lines (thin bands in diffraction patterns) (Fig. 1). To obtain Kikuchi patterns, a sample is placed in a scanning electron microscope so as to make an angle of 70° with the horizontal plane in order to increase the diffraction pattern contrast [15]. Then the sample is exposed to an electron beam. Kikuchi lines are formed as a result of inelastic scattering of electrons reflected from the crystal lattice. Diffraction patterns are recorded on a phosphorescent screen, because tapered beams of diffracted electrons must be visible. A highly sensitive digital CCD camera, connected to a computer for automated determination of crystallographic orientation, is placed behind the screen. The camera is oriented horizontally, so as to approach the phosphorescent screen to the sample and provide a wide capture angle for the diffraction pattern. The areas of intersection of tapered electron beams with the phosphorescent screen manifest themselves in the form of thin bands, referred to as Kikuchi lines [16]. They are brighter than the diffraction pattern background. Indexing of electron backscatter patterns involves assignment of indices to visible bands or intersections of these bands, which are referred to as zones. Zones correspond to the crystallographic directions in crystal. As an example, some of them are highlighted in Fig. 1. A change in the sample lattice orientation in space should change the diffraction patterns. Special computer programs are used to determine automatically the position of each line, perform a comparison with theoretical data on the corresponding crystalline phase, and calculate the three-dimensional crystallographic orientation. Kikuchi line indexing is performed using the corresponding mathematical apparatus (Hough transform) [16].

HKL Channel 5 Software

The coordinate system (Fig. 2). The software works with the following coordinate systems: CSm or X_m, Y_m, Z_m (microscope), which is determined by the microscope axes (this coordinate system is related to the microscope walls); CS1 or X_1, Y_1, Z_1 (data collection surface), which is determined by the axes of measured sample surface (from the perpendicular edges of the angle); CS2 (crystal coordinate system), which is determined by the axes of the crystal unit cell, for example, the crystallographic directions [100], [010], and [001]; CS3 or X_3, Y_3, Z_3 (detector), which is determined by the detector/diffraction pattern (the points in the imaged diffraction pattern are described by the X and Y axes, and the Z axis indicates to the phosphor; and CS0, which is related to the scanning direction and the sample holder surface. An experimental sample was glued to the holder so that the selected direction on the sample was strictly vertical or horizontal; i.e., CS0 and CS1 coincide. The selected direction on the sample may be, e.g., the rolling direction [17]. The Euler angles, which will be used below to calculate the crystallographic parameters, relate the coordinate systems of the crystal unit cell and the sample.

Software capabilities. The HKL Channel 5 software package is designed for the analysis and display of electron backscattered diffraction data. Each program module performs a certain task. The Tango software module serves to form a wide variety of misorientation maps. This software is aimed at generating, displaying, and measuring a set of maps based on electron backscattered diffraction data.

The misorientation angle and rotation axis (misorientation profile) are measured along a Kikuchi line (Figs. 3, 4). When calculating the axis–angle pair in this software, the formulas in use are identical to those applied to construct rotation matrices. Depending on the crystal symmetry, there are different crystallographically equivalent rotation axis–misorientation

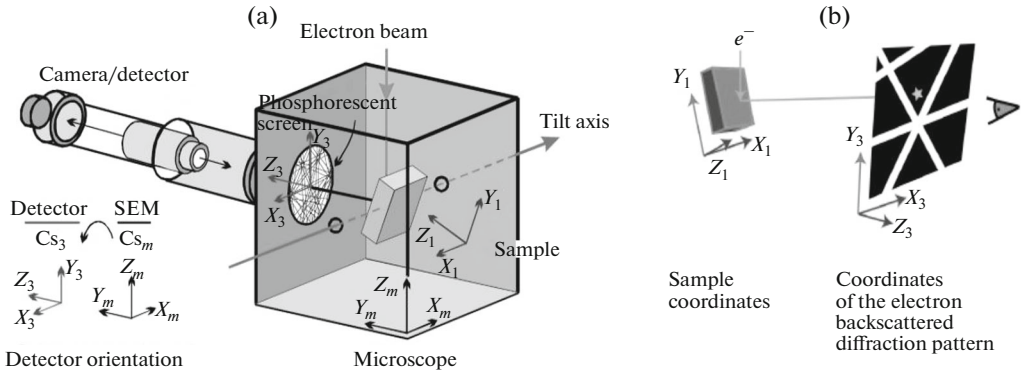

Fig. 2. Coordinate systems in the electron backscattered diffraction method: (a) general description of the coordinate system and (b) the coordinate system of the sample and detector [17].

angle pairs for describing this rotation (for example, 24, 12, and 6 for the cubic, hexagonal, and trigonal symmetries, respectively). Generally, axis–angle pairs with the smallest misorientation angle are used [17]. In other words, an unambiguous representation of orientation in the Rodriguez (axis–angle) space from many equivalent orientations is achieved by choosing the minimum rotation angle, while the rotation axis should lie in the Rodriguez space region determined by the sample symmetry [18]. For example, special GBs making a tilt angle of 70° with the rotation axis [110] and a twist angle of 60° with the axis [111] are considered as crystallographically equivalent.

In addition, the HKL Channel 5 software is applied to calculate the Miller indices of crystallographic planes by transformation of Euler angles [14, 16]. To this end, the normalized vector is converted into an integer vector (the vector computation may be hindered because of incorrect addition to integers). Another important function is to determine the type of special boundaries. The corresponding software includes a library for cubic crystals (a table of correspondence of misorientation angles and rotation axes with the magnitude and reciprocal density of coinciding sites, $\sum$).

Method for Calculating the Rotation Matrix in the Spyder Integrated Environment for Analyzing Crystallographic Parameters

The crystal unit-cell orientation is described relative to a given (laboratory) coordinate system, which is tied to the microscope table (sample holder). In the program settings (HKL Channel 5 software), an orthogonal coordinate system is chosen, which includes the normal direction (ND), rolling direction (RD), and transverse direction (TD). Furthermore, the Euler angles are introduced in the virtual chamber of scanning electron microscope so as to make the coordinate system of the sample holder surface coincide with the sample coordinate system.

Description of Orientation Using Euler Angles

After setting the coordinate systems of the sample and crystal, the orientation is defined as the position of the crystal coordinate system relative to the sample coordinate system:

$$C_c = \mathbf{g}C_s, \tag{1}$$

where C_c is the coordinate system of crystal unit cell; C_s is the sample coordinate system; and $\mathbf{g}$ is the orientation, which can be expressed in several ways. The most general description of orientation or rotation is a 3×3 matrix, which consists of nine direction cosines, linking the three axes of one coordinate system with the three axes of the other system [19, 20]:

$$\mathbf{G} = \begin{bmatrix} a_{11} & a_{12} & a_{13} \\ a_{21} & a_{22} & a_{23} \\ a_{31} & a_{32} & a_{33} \end{bmatrix} = [\mathbf{a}_{ij}]. \tag{2}$$

The first row of the matrix contains the cosines of the angles between the first crystal axis [100] and each of the sample three axes, X, Y, and Z, respectively. The second row contains the cosines of the angles between the [010] crystal axis and each of the three sample axes: X, Y, and Z. Similarly, the third row of the matrix contains the cosines of the angles between the [001] axis and each of the X, Y, and Z axes. The matrix columns are three other unit vectors: the direction cosines for RD, TD, ND in the crystal coordinate system (RD is parallel to the crystal direction $\langle uvw \rangle$, and $\langle hkl \rangle$ is the normal to the crystal plane oriented parallel to the sample plane normal) [20]. The basis vectors of the reference frame, which are associated with the sample, are chosen to be parallel to RD, TD, ND, while the basis vectors associated with the crystal lattice are chosen to be parallel to the [100], [010], and [001] directions.

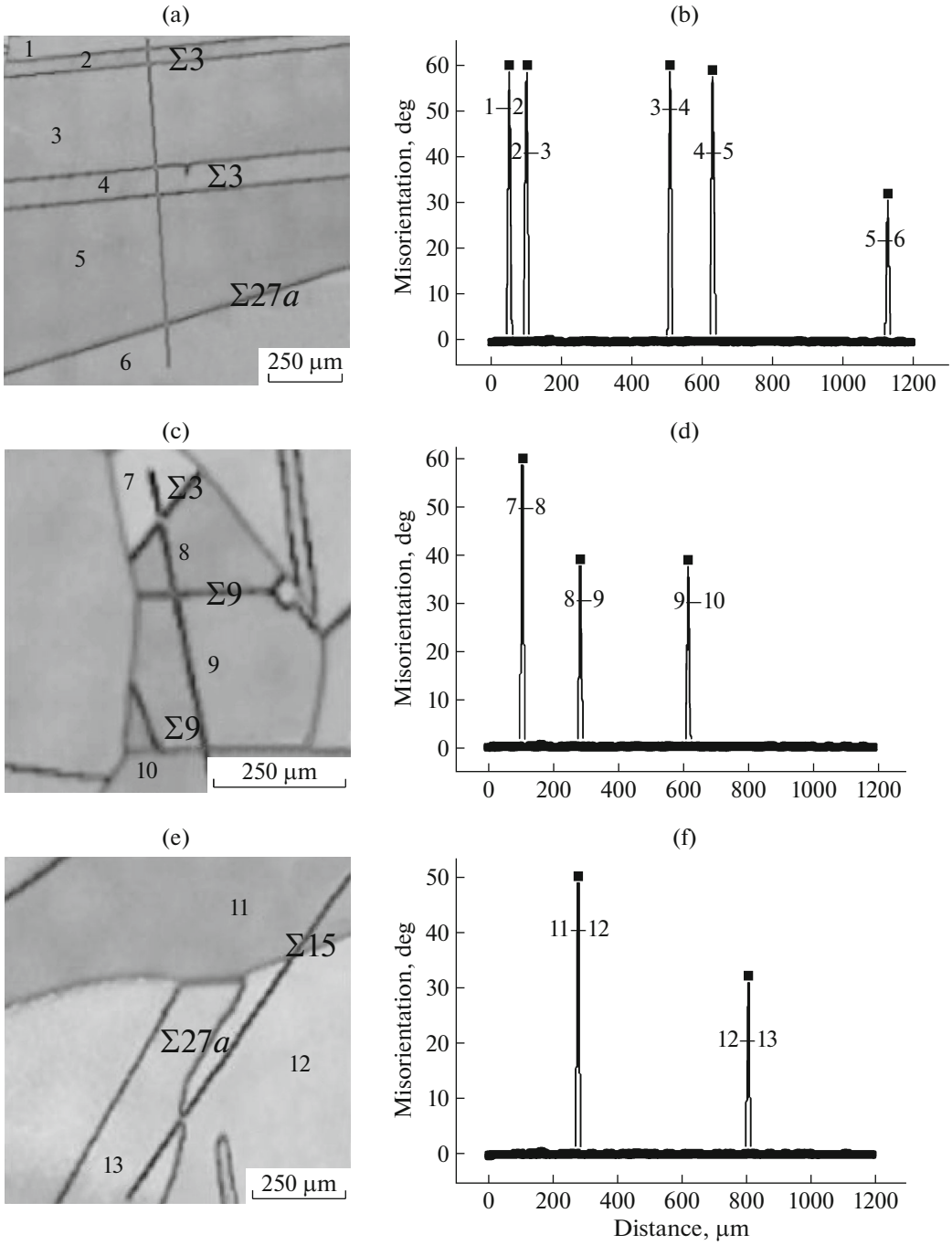

Fig. 3. Measurement of the misorientation profile of areas *1–3*: (a, c, e) fragments of maps for determining the special boundary type (b, d, f) misorientation profiles for selected areas.

The same matrix can be presented as a sequence of three rotations around the main axes (one rotation per axis). The order of the operations described by the formula means that all three Cartesian basis vectors are first rotated by an angle φ_1 around the z axis; then by an angle Φ around the new x axis; and, finally, by an angle φ_2 around the updated z axis [21].

The rotation around the z axis in the matrix representation ($z = z'$) is

$$\mathbf{g}_{\varphi_1}^{z'} = \begin{bmatrix} \cos\varphi_1 & \sin\varphi_1 & 0 \\ -\sin\varphi_1 & \cos\varphi_1 & 0 \\ 0 & 0 & 1 \end{bmatrix}. \quad (3)$$

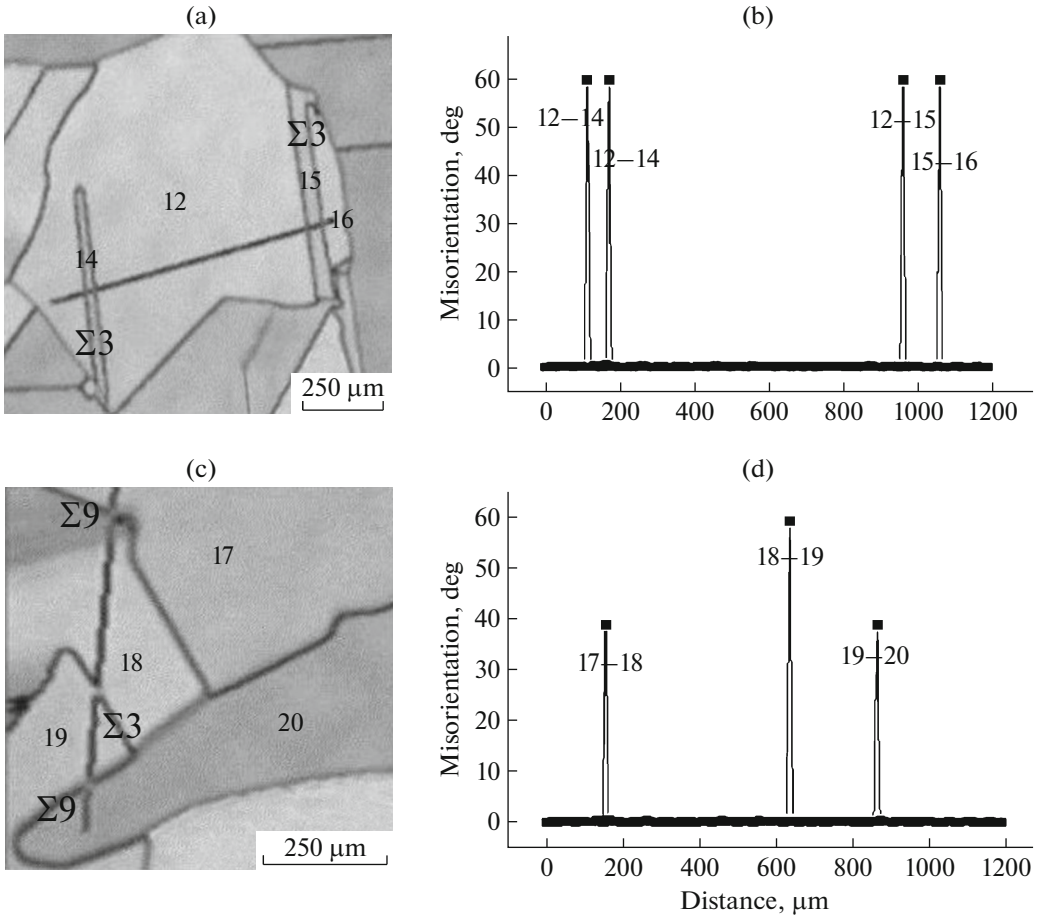

Fig. 4. Measurement of the misorientation profile of areas *4* and *5*: (a, c) fragments of maps for determining the special boundary type and (b, d) misorientation profiles for selected areas.

The rotation around the x axis in the matrix representation ($x = x'$) is

$$\mathbf{g}_{\Phi}^{x'} = \begin{bmatrix} 1 & 0 & 0 \\ 0 & \cos\Phi & \sin\Phi \\ 0 & -\sin\Phi & \cos\Phi \end{bmatrix}. \quad (4)$$

The rotation around the z axis in the matrix representation ($z = z'$) is

$$\mathbf{g}_{\varphi_2}^{z'} = \begin{bmatrix} \cos\varphi_2 & \sin\varphi_2 & 0 \\ -\sin\varphi_2 & \cos\varphi_2 & 0 \\ 0 & 0 & 1 \end{bmatrix}. \quad (5)$$

After three successive rotations,

$$\mathbf{g}(\varphi_1, \Phi, \varphi_2) = \mathbf{g}_{\varphi_1}^{z'}\mathbf{g}_{\Phi}^{x'}\mathbf{g}_{\varphi_2}^{z'}, \quad (6)$$

$$\mathbf{g}(\varphi_1, \Phi, \varphi_2) = \begin{bmatrix} \cos\varphi_1\cos\varphi_2 - \sin\varphi_1\sin\varphi_2\cos\Phi & \sin\varphi_1\cos\varphi_2 + \cos\varphi_1\sin\varphi_2\cos\Phi & \sin\varphi_2\sin\Phi \\ \cos\varphi_1\sin\varphi_2 - \sin\varphi_1\cos\varphi_2\cos\Phi & -\sin\varphi_1\sin\varphi_2 + \cos\varphi_1\cos\varphi_2\cos\Phi & \cos\varphi_2\sin\Phi \\ \sin\varphi_1\sin\Phi & -\cos\varphi_1\sin\Phi & \cos\Phi \end{bmatrix}. \quad (7)$$

Description of the Orientation through a Misorientation Angle–Rotation Axis Pair

The same crystal orientation can be achieved if the crystal coordinate system is rotated by a single angle, provided that the rotation is performed around a certain axis. This angle and axis are known as the misorientation angle and rotation axis, or, briefly, the angle–axis pair [20]. Thus, a three-dimensional rotation, denoted as $\mathbf{g}(\hat{\mathbf{r}}, \Theta)$, can also be given by rotation axis $\hat{\mathbf{r}}$ and rotation angle Θ. Figure 5 shows schematically the angle–axis pair for two coordinate systems of crystals belonging to the cubic system. The left cube is chosen as the starting position, and the right cube must be rotated by 50° around the [001] axis. Let us consider

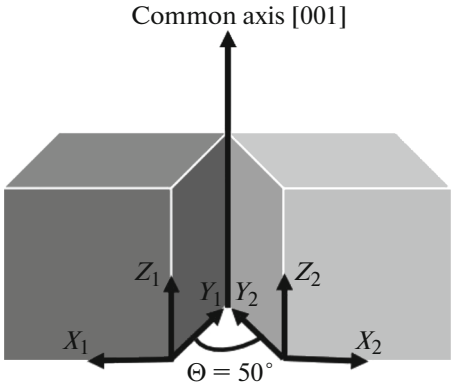

Fig. 5. Two cubic coordinate systems with rotation axis [001] and a misorientation angle of 50°.

the orientation of crystal lattices: x_1, y_1, and z_1 are replaced with a reference coordinate system (e.g., RD, TD, and ND), while X_2, Y_2, and Z_2 are replaced with the crystal axes [100], [010], and [001] [19, 22]:

$$g(\hat{\mathbf{r}},\Theta) = \cos\Theta\begin{bmatrix}1&0&0\\0&1&0\\0&0&1\end{bmatrix} + (1-\cos\Theta)\begin{bmatrix}r_1^2 & r_1r_2 & r_1r_3\\ r_2r_1 & r_2^2 & r_2r_3\\ r_3r_1 & r_3r_2 & r_3^2\end{bmatrix} + \sin\Theta\begin{bmatrix}0 & -r_3 & r_2\\ r_3 & 0 & -r_1\\ -r_2 & r_1 & 0\end{bmatrix}$$
$$= \begin{pmatrix} (1-r_1^2)\cos\Theta + r_1^2 & r_1r_2(1-\cos\Theta) - r_3\sin\Theta & r_1r_3(1-\cos\Theta) + r_2\sin\Theta\\ r_1r_2(1-\cos\Theta) + r_3\sin\Theta & (1-r_2^2)\cos\Theta + r_2^2 & r_2r_3(1-\cos\Theta) - r_1\sin\Theta\\ r_1r_3(1-\cos\Theta) - r_2\sin\Theta & r_2r_3(1-\cos\Theta) + r_1\sin\Theta & (1-r_3^2)\cos\Theta + r_3^2\end{pmatrix}. \quad (8)$$

We will use matrix (8) [20, 23] to derive a formula for the rotation angle (since $\hat{\mathbf{r}}$ is a unit vector, $r_1^2 + r_2^2 + r_3^2 = 1$):

$$\begin{aligned}\text{Trace } \mathbf{g}(\hat{\mathbf{r}},\Theta) &= (1-r_1^2)\cos\Theta + r_1^2 + (1-r_2^2)\cos\Theta\\ &+ r_2^2 + (1-r_3^2)\cos\Theta + r_3^2 + 1\\ &+ [\cos\Theta(1-r_1^2+1-r_3^2+1-r_3^2)] = 1 + 2\cos\Theta;\end{aligned} \quad (9)$$

hence,

$$\cos\Theta = \frac{1}{2}(a_{11} + a_{22} + a_{33} - 1). \quad (10)$$

The r_1, r_2, r_3 values can be calculated from the off-diagonal elements of the rotation matrix (8):

$$\mathbf{g} - \mathbf{g}^{\mathrm{T}} = 2\sin\Theta\begin{bmatrix}0 & -r_3 & r_2\\ r_3 & 0 & -r_1\\ -r_2 & r_1 & 0\end{bmatrix}. \quad (11)$$

At the same time, formula (2) yields

$$\mathbf{g} - \mathbf{g}^{\mathrm{T}} = \begin{bmatrix}0 & a_{12}-a_{21} & a_{13}-a_{31}\\ a_{21}-a_{12} & 0 & a_{23}-a_{32}\\ a_{31}-a_{13} & a_{32}-a_{23} & 0\end{bmatrix}, \quad (12)$$

$$\begin{bmatrix}0 & -r_3 & r_2\\ r_3 & 0 & -r_1\\ -r_2 & r_1 & 0\end{bmatrix} = \frac{\mathbf{g}-\mathbf{g}^{\mathrm{T}}}{2\sin\Theta} = \frac{1}{2\sin\Theta} \times \begin{bmatrix}0 & a_{12}-a_{21} & a_{13}-a_{31}\\ a_{21}-a_{12} & 0 & a_{23}-a_{32}\\ a_{31}-a_{13} & a_{32}-a_{23} & 0\end{bmatrix}, \quad (13)$$

$$\begin{cases} r_1 = \dfrac{a_{32}-a_{23}}{2\sin\Theta}\\ r_2 = \dfrac{a_{23}-a_{32}}{2\sin\Theta}\\ r_3 = \dfrac{a_{13}-a_{31}}{2\sin\Theta}. \end{cases} \quad (14)$$

To calculate the rotation matrix bringing the spatial orientation of one cell to the spatial orientation of another cell (Fig. 5), one must rotate cell 1 so as to make the basis vectors of this cell coincide with the axes of the external coordinate system. This transformation is performed by transposing matrix **1**. Then the cell obtained as a result of the previous transformation must be rotated so as to coincide with the spatial orientation of cell **2** by matrix **2** [19]:

$$\mathbf{M}_{12} = \mathbf{g}_1\mathbf{g}_2^{\mathrm{T}}, \quad (15)$$

where $\mathbf{g}_1$ and $\mathbf{g}_2$ are the orientations of the elementary cells of crystals **1** and **2**, respectively. Then the final rotation matrix takes the form

$$\mathbf{M}_{12} = \begin{bmatrix} \cos\varphi_1\cos\varphi_2 - \sin\varphi_1\sin\varphi_2\cos\Phi & \sin\varphi_1\cos\varphi_2 + \cos\varphi_1\sin\varphi_2\cos\Phi & \sin\varphi_2\sin\Phi \\ \cos\varphi_1\sin\varphi_2 - \sin\varphi_1\cos\varphi_2\cos\Phi & -\sin\varphi_1\sin\varphi_2 + \cos\varphi_1\cos\varphi_2\cos\Phi & \cos\varphi_2\sin\Phi \\ \sin\varphi_1\sin\Phi & -\cos\varphi_1\sin\Phi & \cos\Phi \end{bmatrix}$$
$$\times \begin{bmatrix} \cos\varphi_1^*\cos\varphi_2^* - \sin\varphi_1^*\sin\varphi_2^*\cos\Phi^* & \sin\varphi_1^*\cos\varphi_2^* + \cos\varphi_1^*\sin\varphi_2^*\cos\Phi^* & \sin\varphi_2^*\sin\Phi^* \\ \cos\varphi_1^*\sin\varphi_2^* - \sin\varphi_1^*\cos\varphi_2^*\cos\Phi^* & -\sin\varphi_1^*\sin\varphi_2^* + \cos\varphi_1^*\cos\varphi_2^*\cos\Phi^* & \cos\varphi_2^*\sin\Phi^* \\ \sin\varphi_1^*\sin\Phi^* & -\cos\varphi_1^*\sin\Phi^* & \cos\Phi^* \end{bmatrix}^{\mathrm{T}}. \quad (16)$$

Based on rotation matrix (16), the angle–rotation axis pair was calculated (using formulas (9) and (13)) in the Python 3.7 Spyder environment. It is important that the Euler angles for each grain are measured by electron backscattered diffraction using the Tango HKL Channel 5 software module. Thus, the input data are the values of three Euler angles. The output data are the rotation angle (in degrees) and the rotation axis. The program code is given below

```
import numpy as np
import math
print("Vvedite angle")
f1,f,f2,w1,w,w2 = map(float, input(). split())
f1 = math.radians(f1)
f = math.radians(f)
f2 = math.radians(f2)
w1 = math.radians(w1)
w2 = math.radians(w2)
w = math.radians(w)
A = np. array([[math.cos(f1)*math.cos(f2)-math.sin(f1) *math.sin(f2)*math.cos(f), math.sin(f1)*math.cos(f2)+
math.cos(f1)*math.sin(f2)*math.cos(f),math.sin(f2)* *math.sin(f)], [-math.cos(f1)*math.sin(f2)- math.sin(f1)
*math.cos(f2)*math.cos(f),
math.sin(f1)*math.sin(f2)+math.cos(f1)*math.cos(f)*math.cos(f2), math.cos(f2)* *math.sin(f)],
[math.sin(f1)*math.sin(f),-math.cos(f1)*math.sin(f),math.cos(f)]], dtype = float)
print(B.transpose())
B = B.transpose()
C = A.dot(B)
print(C)
print(A)
print(B)
x = C[0][0]
y = C[1] [1]
z = C[2] [2]
t = math.acos((x+y+z-1)/2)
t1 = math.degrees(t)
print(t1)
x1 = C[2] [1]
x2 = C[1] [2]
y1 = C[0] [2]
y2 = C[2][0]
z1 = C[1][0]
z2 = C[0] [1]
C1 = (x1 x2)/(2*(math.sin(t)))
C2 = (y1 y2)/(2*(math.sin(t)))
C3 = (z1-z2)/(2*(math.sin(t)))
print(C1,C2,C3)
```

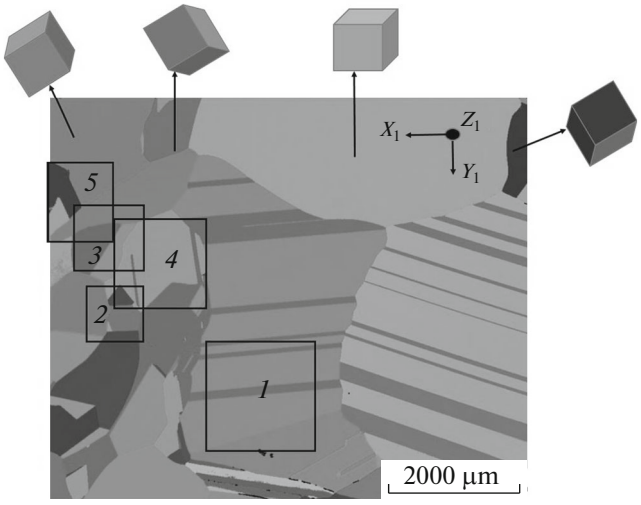

Fig. 6. Orientation map for a multicrystalline silicon sample.

The Miller indices of the crystallographic planes of GBs were also calculated on the basis of the resulting rotation matrix in the Spyder integrated development environment. As was mentioned above, the $\langle hkl \rangle$ indices assign normals to planes. They determine the vector direction cosines and are calculated from the formula [24]

$$\begin{aligned} h &= \sin\Phi\sin\varphi_2, \\ k &= \sin\Phi\cos\varphi_2, \\ l &= \cos\Phi. \end{aligned} \tag{17}$$

RESULTS

Experimental Study by Electron Backscattered Diffraction

The HKL Channel 5 software and electron backscattered diffraction were used to investigate the structural parameters of special-type boundaries in multicrystalline silicon. This particular sample was chosen due to the presence of special GBs of different types in it (∑3, ∑9, ∑27a, ∑15; the reciprocal density of coinciding sites ∑ is the number of metal lattice sites per one coinciding site). The sample surface was prepared for study using grinding and diamond paste polishing.

Table 1. Standard misorientation parameters of special GBs in multicrystalline silicon [7]

Boundary type	Misorientation angle, deg	Rotation axis
∑3	60	[111]
∑3	70.5	[011]
∑9	38	[110]
∑27a	31	[110]

Figure 6 shows an orientation map for a multicrystalline silicon sample. Different colors correspond to different orientations (colors can be selected manually in the program). Euler angles are transformed into colors according to the following formulas [14] (17):

$$\begin{aligned} \text{Red} &= 255\frac{\varphi_1}{360^\circ}, \quad \text{Green} = 255\frac{\Phi}{90^\circ}, \\ \text{Blue} &= 255\frac{\varphi_2}{90^\circ}. \end{aligned} \tag{18}$$

Grain misorientation maps are constructed point by point.

To compare the parameters of special grain boundaries that were calculated using the program and obtained based on rotation matrix calculation, we selected areas *1*–*5* (Fig. 6), which cover various types of the special GBs under study. The misorientation profile displays small changes in the misorientation angle in dependence of the distance between grains. As can be seen in Figs. 3 and 4, all the GBs ∑3, ∑9, and ∑27a are characterized by angles of 58°–60°, 39°–40°, and 31°–32°, respectively. No other versions of crystallographic parameters were detected in measurements; the maximum misorientation angle displayed by the program was 60°. The most abundant special boundaries are ∑3 (they make up about 57% of all special boundaries in the multicrystalline silicon grown by the Bridgman method from UMG-Si).

Table 2. Crystallographic parameters of special GBs for crystals of cubic system [9]

Boundary type	Misorientation angle, deg	Rotation axis
∑3	60	[111]
∑3	180	[1$\bar{2}$1]
∑3	70	[1$\bar{1}$0]
∑3	131	[201]
∑3	146	[3$\bar{1}$1]
∑9	38	[110]
∑9	160	[315]
∑9	123	[$\bar{2}$31]
∑9	120	[511]
∑9	152	[401]
∑9	67	[3$\bar{1}$1]
∑9	180	[2$\bar{2}$1]
∑9	152	[232]
∑9	90	[122]
∑9	96	[012]
∑9	180	[$\bar{1}$14]

Table 3. Comparison of the crystallographic parameters of special grain boundaries in multicrystalline silicon obtained using the HKL Channel 5 software and by our calculations of Euler angles based on experimental electron backscattered diffraction data

Boundary type	Grain no.	Euler angles			Miller indices *hkl*		Misorientation angle Θ, deg		Rotation axis		Boundary variety
		Φ1	Φ	Φ2	program	calculation	program	calculation	program	calculation	
Σ3	1	130.1	45.7	24.8	255	122	60	70.2	$[11\bar{1}]$	[110]	Tilt
	2	211.0	28.3	8.3	012	012					
Σ3	2	211	28.3	8.3	012	012	59.9	70.2	$[11\bar{1}]$	[110]	Tilt
	3	129.8	45.8	25.0	122	122					
Σ3	3	129.8	45.8	25.0	122	122	60	70.2	$[11\bar{1}]$	[110]	Tilt
	4	210.8	28.3	8.3	012	012					
Σ3	4	210.8	28.3	8.3	012	012	60	70.2	$[11\bar{1}]$	[110]	Tilt
	5	130.3	46.1	24.3	255	122					
Σ27a	5	130.3	46.1	24.3	255	122	31.9	31.7	[101]	[110]	Mixed
	6	84.7	43.3	57.5	536	234					
Σ3	7	312.9	38.3	36.4	346	111	59.7	180	$[1\bar{1}\bar{1}]$	$[\bar{1}\,\bar{1}2]$	Tilt
	8	172.3	12	31.3	116	001					
Σ9	8	172.3	12	31.3	116	001	39.4	39	$[0\bar{1}\bar{1}]$	$[0\bar{1}\bar{1}]$	Tilt
	9	118.7	32.4	53.6	326	113					
Σ9	9	118.7	32.4	53.6	326	113	39	40	[011]	[011]	Mixed
	10	175.1	12.2	28.3	116	001					
Σ15	11	206	33.5	42.6	112	112	50.1	76	$[02\bar{1}]$	[112]	Tilt
	12	283.1	39.2	41.9	335	112					
Σ27a	12	283.1	39.2	41.9	335	112	31.2	165	[101]	[112]	Tilt
	13	68.6	51.7	42.8	566	111					
Σ3	12	283.1	39.2	41.9	335	112	59.7	180	$[1\bar{1}1]$	[112]	Tilt
	14	97.7	31.4	48.1	225	113					
Σ3	15	97.2	31.3	48.8	225	113	59.7	180	$[1\bar{1}1]$	[112]	Tilt
	16	283.1	39.3	41.8	335	112					
Σ9	17	338.3	20.7	58.5	216	115	38	120	[011]	[115]	Mixed
	18	105.4	9.7	51.1	116	001					
Σ3	18	105.4	9.7	51.1	116	001	58.9	70	$[1\bar{1}1]$	[011]	Mixed
	19	174.6	51.5	38.9	455	111					
Σ9	19	174.6	51.5	38.9	455	111	40	38	[011]	[011]	Mixed
	20	206	33.5	42.6	112	112					

Results of Calculating the Crystallographic Parameters of Special Boundaries

According to the data in the literature, there is a standard set of misorientation parameters (misorientation angle and rotation axis) of the special GBs under study (Table 1) [7, 12–14]. However, the recent numerical simulation of special GBs for the crystals belonging to the cubic system (hexaoctahedral symmetry class) made it possible to establish versions of misorientation angles and rotation axes for each type of special GBs with a certain ∑ value (Table 2) [9]. The crystallographic parameters obtained by numerical simulation differ from the experimental data reported in the literature. A comparison of the data from Tables 1 and 2 shows that, along with the values given in the literature for special grain boundaries, there are other versions of structural parameters, both for special boundaries ∑3 and ∑9.

Table 3 contains the crystallographic parameters found using the HKL Channel 5 software and obtained by rotation matrix calculation (see above). Despite the use of identical formulas, the parameters of the majority of the boundaries listed in Table 3 do

not coincide with each other and differ from the reference data. For example, a misorientation angle of 180° and the rotation axis [112] were revealed for the boundaries ∑3, and a misorientation angle of 120° and the rotation axis [115] were established for the boundaries ∑9. It is possible that one of the parameters (either the tilt or twist parameter) is used in software-based calculations. However, some specific features of a boundary are not obvious when only the smallest parameter is taken into account. The set of Miller indices of crystallographic GBs planes must be a triad of integers. When calculating this crystallographic parameter from formula (17), one obtains fractional indices (for example, ⟨0.39 0.40 0.83⟩ for grain 20), which must be supplemented to integers.

In particular, in the boundaries of grains 3–4 and 4–5 (Table 3), the Euler angles for grains 3 and 5 differ by only several tenths of degree, but the Miller indices are different.

CONCLUSIONS

Versions of special grain boundaries in multicrystalline silicon grown by Bridgman directional solidification from UMG-Si were identified using electron backscattered diffraction. Since the special grain boundaries present in the same material or sample and belonging to the same type (for example, boundaries ∑3) may exhibit different properties (e.g., recombination activity), the suggestion of differences in their structure or formation nature appears to be quite reasonable [8]. Proceeding from these considerations, all main crystallographic parameters of the GBs under study were calculated, and, correspondingly, the expected differences were established. Specifically, rotation matrix construction was used to determine the crystallographic parameters of special boundaries, which turned out to be consistent with the theoretical data obtained by numerical simulation for a set of cubic crystals but had not been revealed in previous experiments with multicrystalline silicon.

The structural features of special GBs are an important factor in the study of the properties of polycrystalline materials, since these boundaries are the main defects determining the material quality. Therefore, depending on the type and variety, particular boundaries exhibit different properties and, correspondingly, differently affect the properties of material. For example, among the set of boundaries ∑3 in multicrystalline silicon, there may be significant differences in the degree of recombination activity exhibited by boundaries of this type. However, the database of the most popular method for studying the misorientation parameters and determining the types of grain boundaries (electron backscattered diffraction) contains not all special boundary parameters that are likely for multicrystalline silicon, a fact significantly reducing the quality of research results and conclusions drawn in the field of materials science.

FUNDING

This study was supported by a State contract (project no. IX.125.3.2).

REFERENCES

1. J. Benick, A. Richter, R. Muller, and H. Hauser, IEEE J. Photovoltaics B **7** (5), 1171 (2017).
2. V. Osinniy, P. Bomholt, A. Nylandsted Larsen, et al., Solar En. Mater. Solar Cells B **95** (2), 564 (2011).
3. H. Ch. Sio, S. Ph. Phang, T. Trupke, et al., IEEE J. Photovoltaics B **5** (5), 1357 (2015).
4. K. Adamczyk, R. Sondena, G. Stokkan, et al., J. Appl. Phys. B **123** (5), 055705 (2018).
5. J. Chen, T. Sekiguchi, D. Yang, et al., J. Appl. Phys. B **96** (10), 5490 (2004).
6. B. Chen, J. Chen, T. Sekiguchi, et al., J. Appl. Phys. B **105** (11), 113502 (2009).
7. R. R. Prakash, Ph. D. Thesis (Univ. of Tsukuba, Tsukuba, Japan).
8. S. M. Peshcherova, E. B. Yakimov, A. I. Nepomnyashchikh, et al., Semiconductors **49** (6), 724 (2015).
9. A. J. Morawiec, Appl. Cryst. B **44**, 1152 (2011).
10. A. J. Morawiec, Mater. Sci. Forum. B **702–703**, 697 (2012).
11. V. Yu. Lazebnykh and A. S. Mysovsky, J. Appl. Phys. B **118** (13), 135704 (2015).
12. A. Stoffers, O. Cojocaru-Miredin, W. Seifert, et al., Prog. Photovoltaics Res. Appl. B **23** (12), 1742 (2015).
13. G. Stokkan, A. Stoss, M. Kivambe, et al., *28th European Photovoltaic Solar Energy Conference and Exhibition B* (2013), p. 14.
14. L. Chuang, K. Maeda, H. Morito, et al., Scr. Mater. B **148**, 37 (2018).
15. M. L. Lobanov, A. S. Yurovskikh, N. I. Kardonina, and G. M. Rusakov, *Methods for Studying Textures in Materials* (Izd-vo Ural'skogo Univ., Yekaterinburg, 2014) [in Russian].
16. A. Shvarts, M. Kumar, B. Adams, and D. Fild, *Method of Reflected Electron Diffraction in Materials Science* (Tekhnosfera, Moscow, 2014) [in Russian].
17. *Oxford Instrument HKL Technology CHANNEL 5: User Manual* (Hobro, Denmark, 2007), p. 475.
18. S. M. Mokrova, R. P. Petrov, and V. N. Milich, Vestn. Udmurt. Univ.: Mat. Mekh. Comp'ut. Nauki **26** (3), 336 (2016).
19. A. V. Tverdokhlebova, Candidate's Dissertation in Physics and Mathematics (IFPM SO RAN, Tomsk, 2017).
20. O. Engler and V. Randle, *Introduction to Texture Analysis: Macrotexture, Microtexture, and Orientation* (Taylor and Francis, 2009), p. 488.
21. H.-J. Bunge, *Texture Analysis in Materials Science* (Institut fur Metallkunde und Metallphysic, Technische Universitat Clausthal, 1969).
22. J. S. Dai, Mech. Mach. Theor. B **92**, 144 (2015).
23. G. A. Korn and T. M. Korn, *Mathematical Handbook for Scientists and Engineers* (McGraw-Hill, New York, 1968).
24. F. J. Hampherys and M. Hatherly, *Recrystallization and Related Annealing Phenomena* (Univ. of Manchester, Institute of Science and Technology, UK and Univ. of New South Wales, Australia, 2004).

Translated by Yu. Sin'kov